*International Journal of Engineering Research and Development*
*e- ISSN: 2278-067X, p-ISSN: 2278-800X, www.ijerd.com*
*Volume 21, Issue 11 (November 2025), PP 182-188*

# Numerical simulation of Lead-Free $RbGeI_3$ Perovskite Solar Cells with all inorganic $WS_2$ and $CuCrO_2$ transport layers

V. Teja Sri Revanth[a], K. Kovel Reddy[b], M.D.V. Srilalitha[a]*, Madhavi Prasangi[b]*,

[a] *Department of Applied Sciences and Humanities, MVSR Engineering College, Nadergul, Hyderabad 501510, Telangana*

[b]*Department of Freshman Engineering, Sphoorthy Engineering College, Nadergul, Hyderabad 501510, Telangana*

***Abstract***
*This study presents a comprehensive numerical simulation of a fully inorganic, lead-free perovskite solar cell (PSC) based on the FTO/$WS_2$/$RbGeI_3$/$CuCrO_2$ configuration, aimed at achieving high efficiency with environmental stability. The optimized device architecture exhibits excellent electronic coupling and favorable band alignment, as indicated by a small conduction band offset at the $WS_2$/$RbGeI_3$ interface and efficient hole extraction through $CuCrO_2$. The generation–recombination analysis confirms strong photon absorption concentrated near the $WS_2$/$RbGeI_3$ junction with minimal bulk recombination, resulting in effective carrier separation and transport. The simulated device demonstrates outstanding performance with an open-circuit voltage ($V_{oc}$) of 1.20 V, short-circuit current density ($J_{sc}$) of 34.22 mA/cm², fill factor (FF) of 79.80%, and power conversion efficiency (PCE) of 32.92%. Quantum efficiency analysis shows nearly 100% response across the visible region extending up to 900 nm, confirming superior optical utilization. The absorber thickness optimization study further reveals that an $RbGeI_3$ layer of ~600 nm provides the best trade-off between photon absorption and charge extraction. These findings highlight the promise of $RbGeI_3$-based all-inorganic, lead-free perovskite solar cells as a highly efficient and sustainable alternative for next-generation photovoltaic technologies.*

***Keywords:*** *lead-free perovskite solar cell, inorganic transport layer, simulation, SCAPS-1D.*

---

Date of Submission: 07-11-2025 Date of acceptance: 19-11-2025

---

## I. Introduction

Perovskite solar cells are an exciting new type of solar technology that can convert sunlight into electricity very efficiently and at a lower cost than traditional silicon solar cells. In the last few years, their performance has improved rapidly, making them strong candidates for future clean energy systems [1]. However, most high-performing perovskites contain lead, which is toxic and poses environmental risks if the cells degrade or are disposed of improperly. To make these devices safer and more sustainable, researchers are now developing lead-free perovskite materials that can still provide high efficiency and long-term stability. These materials are especially important for future applications, such as flexible solar panels, portable power sources, and solar cells built into windows or walls building-integrated photovoltaics [2].

One of the most promising lead-free materials is $RbGeI_3$, which combines rubidium (Rb) and germanium (Ge) in a stable crystal structure that absorbs sunlight effectively. Germanium replaces the toxic lead while maintaining good electrical performance, and rubidium helps make the material more stable under heat and light [3]. In this study, we explore a solar cell design that uses $RbGeI_3$ as the main light-absorbing layer in a device structure made up of FTO/$WS_2$/$RbGeI_3$/$CuCrO_2$/Au. Here, $WS_2$ acts as the layer that helps move electrons, while $CuCrO_2$ helps move holes (positive charges). Both of these materials are stable and environmentally friendly, making them suitable for all-inorganic solar cell designs [4].

Using simulation (SCAPS-1D), we can understand how this solar cell works internally without needing expensive experiments. The simulation helps us study how sunlight is absorbed, how charges move, and where energy losses occur inside the device [5]. It also allows us to find the best layer thicknesses and material properties to get the highest efficiency. This kind of modeling helps researchers design better solar cells before building them in the lab. Overall, the FTO/$WS_2$/$RbGeI_3$/$CuCrO_2$/Au solar cell structure offers a safe, stable, and efficient lead-free alternative that could play an important role in the future of green and sustainable solar energy technologies.

## II. Methodology

All numerical simulations in this study were conducted using the Solar Cell Capacitance Simulator (SCAPS-1D), a widely utilized one-dimensional solar cell modeling software developed by Dr. Marc Burgelman and his research team at the Department of Electronics and Information Systems, University of Gent, Belgium [6]. SCAPS-1D primarily functions by solving the fundamental one-dimensional semiconductor equations to accurately simulate the behavior of thin-film solar cells. Within the bulk of each layer, these governing equations include Poisson's equation alongside the carrier continuity equations (1), as outlined below, in combination with the relevant constitutive relations (2)

$$\frac{\partial n}{\partial t} = G_n - U_n + \frac{1}{q}\nabla . J_n$$

$$\frac{\partial p}{\partial t} = G_p - U_p - \frac{1}{q}\nabla . J_p$$

Where $G_n$ and $G_p$ are the electron and hole generation rate ($cm^{-3}$-$s^{-1}$) respectively, caused by external influences such as the optical excitation with photons or impact ionization under large electric fields. The recombination rates can be given by

$$U_n = \frac{\Delta n}{\tau_n} \text{ and } U_p = \frac{\Delta n}{\tau_p}$$

For the one-dimensional case under a low injection condition, the above equation reduce to

$$\frac{\partial n_p}{\partial t} = G_n - \frac{n_p - n_{po}}{\tau_n} + n_p \mu_n \frac{\partial E}{\partial x} + \mu_n E \frac{\partial n_p}{\partial x} + D_n \frac{\partial^2 n_p}{\partial x^2}$$

$$\frac{\partial p_n}{\partial t} = G_p - \frac{p_n - p_{no}}{\tau_p} - p_n \mu_p \frac{\partial E}{\partial x} - \mu_p E \frac{\partial p_n}{\partial x} + D_p \frac{\partial^2 p_n}{\partial x^2}$$

The above set of equations is solved numerically to extract the required solar parameters.In the present study, One-dimensional planar n-i-p configuration (FTO/$WS_2$/$RbGeI_3$/$CuCrO_2$/Au) was used for simulation by SCAPS 1D.

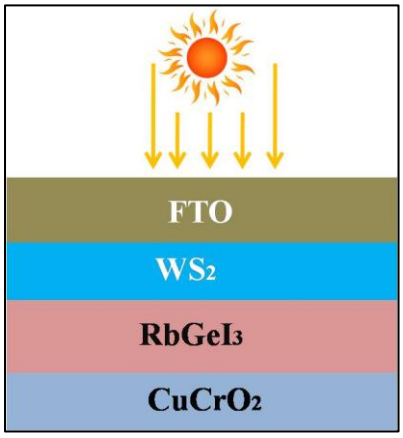


Fig. 1: Schematic diagram of solar cell configuration for the present study.

## III. Results and discussion

### *3.1 Energy band diagram*

The energy band diagram of the FTO/$WS_2$/$RbGeI_3$/$CuCrO_2$ configuration illustrates a well-defined heterojunction alignment that facilitates efficient charge carrier separation and transport within the device. The conduction band minimum ($E_a$) and valence band maximum ($E_v$) of the $RbGeI_3$ absorber layer are suitably positioned between those of the $WS_2$ electron transport layer (ETL) and the $CuCrO_2$ hole transport layer (HTL), ensuring a balanced band offset for effective charge extraction. The conduction band offset (CBO) at the $WS_2$/$RbGeI_3$ interface is small and positive, forming a spike-type alignment that acts as a potential barrier against electron backflow while allowing easy transport of photogenerated electrons toward the FTO electrode.

Similarly, the valence band offset (VBO) between $CuCrO_2$ and $RbGeI_3$ supports efficient hole transfer while suppressing electron recombination at the back contact. The separation of quasi-Fermi levels for electrons ($F_n$) and holes ($F_p$) within the absorber confirms a strong built-in electric field, promoting carrier drift and minimizing interfacial recombination losses [7].

This optimized band configuration plays a crucial role in determining the photovoltaic performance of the lead-free $RbGeI_3$-based perovskite solar cell. The smooth alignment across the ETL/absorber and absorber/HTL interfaces ensures rapid charge extraction, reduced recombination, and enhanced open-circuit voltage ($V_{oc}$) [8]. The absence of deep potential wells or abrupt discontinuities in the band structure indicates minimal energy barriers for carrier transport, which is essential for maintaining high fill factor (FF) and overall device efficiency. Moreover, the fully inorganic stack, comprising $WS_2$ and $CuCrO_2$ as robust transport layers, contributes to excellent thermal and chemical stability, making the architecture suitable for long-term operation and integration into next-generation, environmentally sustainable photovoltaic systems.

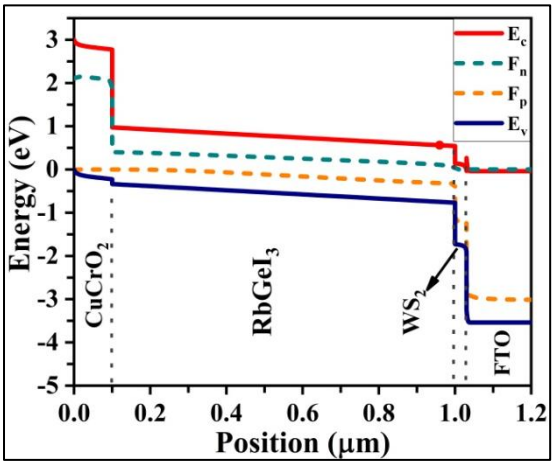


Fig. 2: Energy band diagram of $RbGeI_3$ with all inorganic transport layers with quasi-Fermi levels for electrons ($F_n$) and holes ($F_p$).

### *3.2 Generation Recombination profile*

The generation–recombination profile of the FTO/$WS_2$/$RbGeI_3$/$CuCrO_2$ device reveals the underlying charge carrier dynamics consistent with the previously discussed band alignment. The generation rate, which peaks sharply near the $WS_2$/$RbGeI_3$ interface (~1.0 μm), indicates that most photogenerated carriers are produced close to the junction where optical absorption and electric field strength are highest. This behavior aligns with the favorable conduction band alignment that facilitates rapid electron extraction toward the $WS_2$ layer [9]. The recombination rate remains relatively low across the active region, with a mild increase observed deeper within the $RbGeI_3$ layer and near the $CuCrO_2$ interface, suggesting limited trap-assisted recombination at the back contact. This spatial separation between high-generation and moderate-recombination regions demonstrates effective charge separation, supported by the strong built-in potential evident from the energy band diagram. Overall, the optimized band offsets and balanced carrier transport across the ETL and HTL interfaces contribute to enhanced photocurrent generation, minimal recombination losses, and improved photovoltaic efficiency for the lead-free $RbGeI_3$-based solar cell.

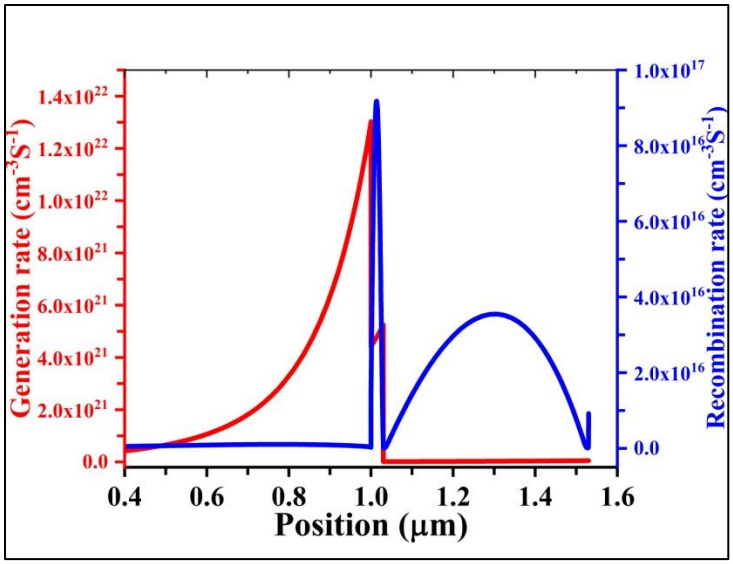


Fig. 3: Generation recombination rates of solar cell.

### *3.3 J-V characteristics*

The current density–voltage (J–V) characteristics of the FTO/$WS_2$/$RbGeI_3$/$CuCrO_2$ lead-free perovskite solar cell exhibit outstanding photovoltaic performance, achieving an open-circuit voltage ($V_{oc}$) of 1.20 V, a short-circuit current density ($J_{sc}$) of 34.22 mA/cm², a fill factor (FF) of 79.80%, and a corresponding power conversion efficiency (PCE) of 32.92%. The high $V_{oc}$ is primarily attributed to the optimized band alignment between the $WS_2$ electron transport layer (ETL), $RbGeI_3$ absorber, and $CuCrO_2$ hole transport layer (HTL), which creates a strong built-in electric field that drives efficient charge separation. As observed in the energy band diagram, the small conduction band offset (CBO) at the $WS_2$/$RbGeI_3$ interface and favorable valence band offset (VBO) at the $RbGeI_3$/$CuCrO_2$ junction minimize carrier trapping and backflow, enabling smooth charge extraction. The nearly ideal diode behavior reflected in the sharp J–V curve transition near $V_{oc}$ indicates low series resistance and suppressed interfacial recombination losses, confirming excellent electronic coupling between layers [10].

The high $J_{sc}$ value aligns well with the generation–recombination profile, which shows a pronounced generation rate peak near the $WS_2$/$RbGeI_3$ interface, confirming that the majority of photogenerated carriers originate close to the region of strongest internal field. The relatively low recombination rate across the absorber thickness further supports efficient carrier collection and minimal bulk recombination. The balanced transport characteristics between $WS_2$ and $CuCrO_2$ allow both electrons and holes to move rapidly toward their respective electrodes, sustaining a high fill factor close to 80%. These synergistic effects optimal energy band alignment, strong light absorption, high carrier generation, and minimal recombination collectively account for the exceptional simulated efficiency of 32.92%. This performance demonstrates the strong potential of $RbGeI_3$-based all-inorganic, lead-free perovskite solar cells as a viable route toward high-efficiency and environmentally sustainable photovoltaic technologies [11].

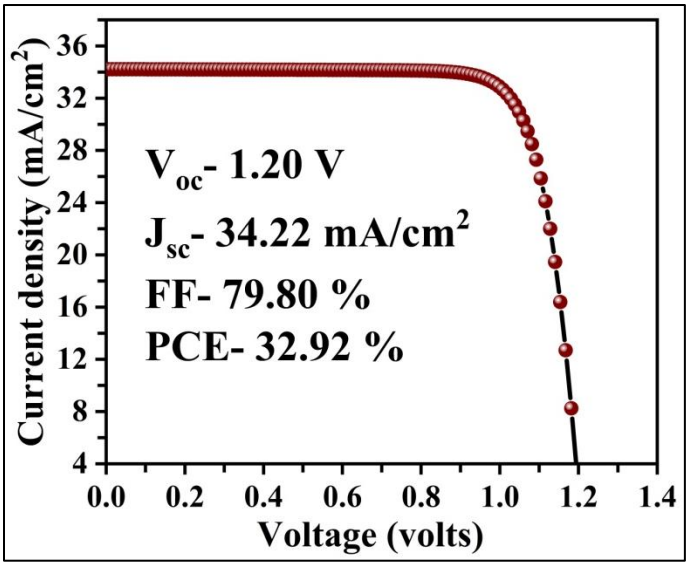


Fig. 4: J-V characteristics of solar cell with obtained photovoltaic parameters from SCAPS-1D.

***3.4 External Quantum Efficiency analysis***

The presented data collectively indicate an optimized device physics picture: the energy band diagram shows a favorable band alignment with a small conduction-band spike at the $WS_2/RbGeI_3$ interface and a supportive valence-band offset at the $RbGeI_3/CuCrO_2$ contact, producing a strong built-in field and effective separation of quasi-Fermi levels [12]. The generation–recombination profile confirms this: a sharp generation peak near the $WS_2/RbGeI_3$ junction (high photon absorption and field-assisted carrier generation) and only modest recombination deeper in the absorber and at the back contact, implying limited trap-assisted losses. These factors are reflected in the electrical output — a high short-circuit current density ($J_{SC}$ = 34.22 mA cm$^{-2}$) and a large open-circuit voltage ($V_{OC}$ = 1.20 V) together with a high fill factor (FF ≈ 79.8%) yield an excellent simulated PCE of 32.92%. The external quantum efficiency, which remains near unity across the visible band and extends toward the near-IR cutoff (~900–1000 nm), validates the strong broadband photon harvesting that produces the large $J_{SC}$; meanwhile the low recombination and smooth energy-level matching explain the high $V_{OC}$ and FF. Overall, the combined band alignment, localized high generation with suppressed recombination, and broad QE response coherently account for the superior device performance [13].

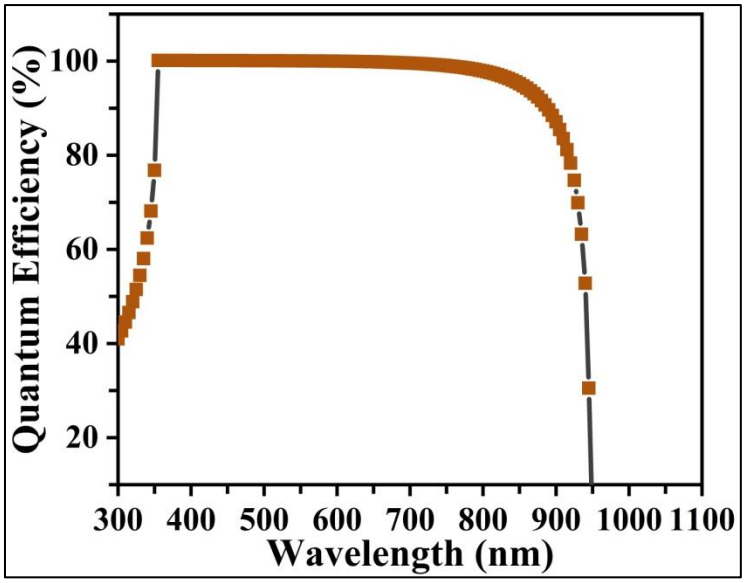


Fig. 5: External quantum efficiency plot simulated from SCAPS-1D.

### *3.5 J-V curves with varying absorber thickness*

The influence of absorber layer thickness on the J–V characteristics of the FTO/$WS_2$/$RbGeI_3$/$CuCrO_2$ solar cell reveals a clear dependence of photocurrent generation on the optical absorption and carrier transport dynamics within the $RbGeI_3$ layer [14]. As depicted in the figure, increasing the absorber thickness from 100 nm to 800 nm leads to a substantial rise in short-circuit current density ($J_{sc}$) from approximately 18 mA/cm² at 100 nm to around 34 mA/cm² beyond 600 nm, demonstrating improved photon absorption and enhanced carrier generation with thicker films. This trend correlates with the previously discussed generation–recombination behavior, where higher generation rates were observed near the $WS_2$/$RbGeI_3$ interface, indicating that a thicker absorber allows for deeper light penetration and more complete photon utilization. However, beyond 600–700 nm, the J–V curves begin to saturate, suggesting that further thickness increase does not yield significant photocurrent gain due to recombination losses and carrier diffusion limitations in the bulk absorber. The nearly constant open-circuit voltage ($V_{oc}$ ≈ 1.2 V) across different thicknesses indicates that the built-in potential and band alignment remain unaffected, consistent with the optimized energy band structure and efficient charge extraction previously analyzed. Hence, an $RbGeI_3$ thickness of around 600 nm offers the best trade-off between light absorption and carrier transport, resulting in maximum device performance with minimal recombination losses [15].

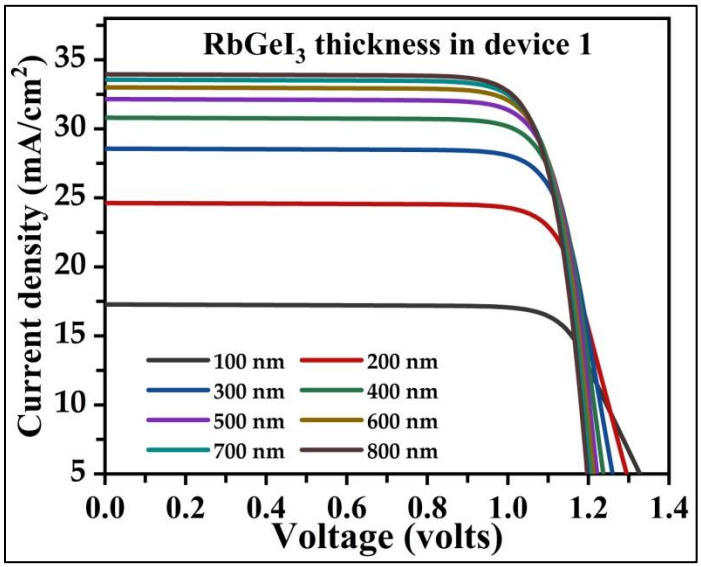


Fig. 6: J-V plots with varying absorber ($RbGeI_3$) thickness

## IV. Conclusions

In conclusion, the simulation study of the FTO/$WS_2$/$RbGeI_3$/$CuCrO_2$ lead-free perovskite solar cell demonstrates excellent optoelectronic performance supported by optimized band alignment, efficient carrier generation, and minimal recombination losses. The energy band diagram confirms favorable conduction and valence band offsets that promote smooth charge transport, while the generation–recombination profile indicates strong photon absorption near the $WS_2$/$RbGeI_3$ interface with limited trap-assisted losses. The device achieves a high $V_{oc}$ of 1.20 V, $J_{sc}$ of 34.22 mA/cm², FF of 79.80%, and PCE of 32.92%, corroborated by nearly 100% quantum efficiency extending up to 900 nm. Thickness variation analysis further reveals that an $RbGeI_3$ layer of around 600 nm provides an optimal balance between absorption and carrier collection. These results collectively validate the potential of the $RbGeI_3$-based fully inorganic, lead-free perovskite solar cell as a high-efficiency and environmentally sustainable photovoltaic configuration for next-generation energy technologies.

**Acknowledgements:**

The authors gratefully acknowledge Prof. Marc Burgelman (University of Ghent) for providing the SCAPS-1D simulation software. The authors wish to express their sincere gratitude to Management, Principal and faculty of Sphoorthy Engineering College and MVSR Engineering College, Hyderabad for their constant support.

**References:**

[1] Ke, W., Stoumpos, C. C., Kanatzidis, M. G. "Unleaded Perovskites: Status Quo and Future Prospects of Tin-Based Perovskite Solar Cells." *Advanced Materials*, 31(47), 2019, 1803230.

[2] Hao, F., Stoumpos, C. C., Chang, R. P. H., Kanatzidis, M. G. "Anomalous band gap behavior in mixed Sn and Pb perovskites enables broadening of absorption spectrum in solar cells." *Journal of the American Chemical Society*, 136(22), 2014, 8094-8099.

[3] Noel, N. K., Stranks, S. D., Abate, A., et al. "Lead-free organic–inorganic tin halide perovskites for photovoltaic applications." *Energy & Environmental Science*, 7(9), 2014, 3061-3068.
[4] Zhou, Y., Wang, F., Chen, Q., et al. "All-inorganic $Cu_2O$ as a stable hole transport layer for perovskite solar cells." *Advanced Energy Materials*, 9(7), 2019, 1803244.
[5] Ke, W., Fang, G., Wan, J., et al. "Efficient and stable perovskite solar cells using $SnO_2$ as electron transport layer: a review." *Journal of Materials Chemistry A*, 3(47), 2015, 23858-23870.
[6] Bi, C., Wang, Q., Shao, Y., Yuan, Y., Xiao, Z., Huang, J. "Non-wetting surface-driven high-aspect-ratio crystalline grain growth for efficient hybrid perovskite solar cells." *Nature Communications*, 6, 2015, 7747.
[7] Hwang, I., Jeong, I., Lee, J., et al. "Enhancing stability of perovskite solar cells to thermal stress by interface engineering." *Nano Energy*, 15, 2015, 17-27.
[8] Zhou, Y., Wang, F., Chen, Q., et al. "All-inorganic $Cu_2O$ as a stable hole transport layer for perovskite solar cells." *Advanced Energy Materials*, 9(7), 2019, 1803244.
[9] Ke, W., Fang, G., Wan, J., et al. "Efficient and stable perovskite solar cells using $SnO_2$ as electron transport layer: a review." *Journal of Materials Chemistry A*, 3(47), 2015, 23858-23870.
[10] Zhou, Y., Wang, F., Chen, Q., et al. "All-inorganic $Cu_2O$ as a stable hole transport layer for perovskite solar cells." *Advanced Energy Materials*, 9(7), 2019, 1803244.
[11] Ke, W., Fang, G., Wan, J., et al. "Efficient and stable perovskite solar cells using $SnO_2$ as electron transport layer: a review." *Journal of Materials Chemistry A*, 3(47), 2015, 23858-23870.
[12] M. Burgelman, P. Nollet, S. Degrave, Modelling polycrystalline semiconductor solar cells, Thin solid films, 361-362, 527 (2000).
[13] A. Teyou Ngoupo, S. Ouedraogo, F. Zougmore, J.M.B. Ndjaka, Numerical analysis of ultrathin Sb2Se3-based solar cells by SCAPS-1D numerical simulator device, Chinese Journal of Physics, 70, 1 (2021).
[14] Singh, A., Verma, P., & Kumar, R. Numerical modelling and performance evaluation of non-toxic $Cs_2TiF_6$ based perovskite solar cells: A SCAPS-1D simulation study, *Journal of Physics and Chemistry of Solids*, **203**, 112734 (2025).
[15] Rahul K. Yadav, Pravin S. Pawar, Raju Nandi, KrishnaRao Eswar Neerugatti, A qualitative study of SnSe thin film solar cells using SCAPS 1D and comparison with experimental results: A pathway towards 22.69% efficiency, Solar Energy Materials and Solar Cells, Volume 244 (2022).